PROCEEDINGS OF SCIENCE

An updated view of the VHE gamma-ray sky around the stellar cluster Westerlund 2 with the H.E.S.S. experiment

Tim Lukas Holch[a,*] **and Emma de Oña Wilhelmi**[a] **for the H.E.S.S. Collaboration**

[a] *Deutsches Elektronen-Synchrotron DESY,*
Platanenallee 6, 15738 Zeuthen, Germany

E-mail: tim.lukas.holch@desy.de, emma.de.ona.wilhelmi@desy.de

Since the last H.E.S.S. publication on the stellar cluster Westerlund 2 in 2011, the H.E.S.S. dataset on this region has increased more than three-fold in exposure to ~ 220 h of total observation time. By applying a novel approach to correct for atmospheric variations in IACT data, the commonly applied data quality selection criteria can be adapted to exploit as much of this dataset as possible. In combination with current analysis techniques, it is furthermore possible to disentangle and better characterise this complex region of the gamma-ray sky. Applying an extensive 3D fitting procedure, we find three distinct VHE gamma-ray sources in the vicinity of Westerlund 2, adding a new emission region to the previously reported sources HESS J1023−575 and HESS J1026−582. Even though the sources partly overlap, their spectral indices differ from one another, providing new clues on the relativistic particle acceleration and propagation in the region around the massive star cluster. The new source component shows an elongated morphology that seems to emerge from the star cluster, following the multi-parsec-scale CO jet cloud initially found in NANTEN data as reported in 2009.

The 38th International Cosmic Ray Conference (ICRC2023)
26 July – 3 August, 2023
Nagoya, Japan

*Speaker

PoS(ICRC2023)778

1. Introduction

The gamma-ray sky around the stellar cluster Westerlund 2 is one of the most intriguing regions on the southern sky. Due to its position on the outer edge of the Carina arm of the Milky Way, various potential cosmic-ray accelerators as well as potential target material cluster along our line of sight. The initial detection of gamma-ray signals > 100 MeV in this region was already reported by the COSB experiment in 1981 [1] with successive detections at GeV energies by the EGRET [2], AGILE [3] and Fermi-LAT [4] experiments. At very high energy ($E > 100$ GeV), gamma-ray emission was first detected by the H.E.S.S. telescope array [5] with a refined analysis published in 2011 where the detection of a second VHE gamma-ray source was presented [6]. Since then, H.E.S.S. has continued to observe the Westerlund 2 region, substantially increasing its exposure at TeV energies. In combination with new techniques to correct for atmospheric variations [7, 8] and multidimensional modelling procedures, it is now possible to describe the emission in this region in unprecedented detail. In this contribution, we present updated spatial and spectral models for the known sources HESS J1023−575 and HESS J1026−582 as well as a newly detected component we here refer to as HESS J1024−583 which shows an elongated morphology in spatial agreement with elongated cloud structures found in HI and CO radio data [9, 10].

2. Data, analysis and results

2.1 Observations and data reduction

The H.E.S.S. telescope array has observed the region around Westerlund 2 from 2006 to 2015 for > 220 h with its four 107 m^2 mirror area (12 m dish diameter) imaging atmospheric Cherenkov telescopes (IACTs) located in the Khomas Highland of Namibia. Besides dedicated observations of the stellar cluster, the dataset also includes observations performed in course of the H.E.S.S. Galactic Plane Survey [11] and observations targeted at the VHE source complex HESS J1018−589 [12].

After data quality selection for hardware performance, the dataset yields a total of 357 observation runs with a total livetime of ∼ 158 h. Air-shower properties are reconstructed for this dataset using a shower image analysis based on Hillas parameters [13] in a configuration that is optimised for high energies in the TeV domain and uses a suppression method for hadronic background events based on boosted decision trees [14]. The reconstructed air-shower properties and according instrument response functions (IRFs) are then exported to fits format according to the GADF (*gamma astro data formats*) [15] which are then analysed using the `gammapy` analysis package [16] in version 1.0.

Before the air-shower data is reduced into a data cube structure, the reconstructed shower energies are corrected for estimated average atmospheric aerosol conditions during the individual observations as outlined in more detail in [7] and [8]. The atmosphere corrected gamma-ray data and IRFs are then stacked into a data cube structure with ten evenly log-spaced energy bins from 0.8 TeV to 85 TeV and spatial bins of $0.02° \times 0.02°$ centred around the core of the studied gamma-ray source complex at 284.5° galactic longitude and −0.5° galactic latitude. Furthermore, a selection cut is applied at 15% energy-bias to improve the accuracy of reconstructed shower energies. The background model is generated by applying the so-called adaptive ring background

estimation technique [17] in each of the ten energy bins, shielding the regions of known and apparent gamma-ray excess.

2.2 3D fit and model selection procedure

To generate a detailed spatial and spectral description of the detected TeV emission, an extensive so-called 3D fitting procedure in `gammapy` is performed. In this procedure, spatial and spectral properties of model components are concurrently optimised by minimising the `cash` statistic[1] of the model and the observed data. A *preferred* model is eventually selected from a collection of tested candidate models using the Akaike information criterion (AIC), a concept from the domain of information theory initially proposed by Hirotogu Akaike in 1973 [18]. The AIC estimates the Kullback-Leibler divergence between a given model and the underlying generating distribution of the observed data[2]. It can thus be used to rank the models in the candidate collection by the amount of information which is lost when using them to describe the observed data. The AIC score of a model is defined as

$$\mathrm{AIC} = -2 \ln f(D|\hat{\theta}_p) + 2p \tag{1}$$

where $f(D|\hat{\theta}_p)$ is the likelihood of observing the data D, assuming a model with its p free best-fit parameters $\hat{\theta}_p$. The first term is determined by the maximum likelihood fit (in the case of a 3D fit using `gammapy` this is simply the `cash` statistic value for the model with its best-fit parameters and the data), while the second term is a penalty for model complexity. The model with the lowest AIC score can in general be regarded as being preferred from all models in the candidate collection as it yields the best description of the observed data using an adequate number of free model parameters. If two models, however, have a difference in AIC of < 2, these are commonly regarded as describing the observed data equally well [19].

To find a model that describes the observed emission with an adequate number of parameters, i.e. without under- or over-fitting the data, the models of the candidate collection should cover a range of complexity with different numbers of free model parameters, enough to capture a point where higher model complexity does no longer reduce the AIC score. It is also important to remember that the AIC only ranks the tested candidate models, and thus helps to decide which of the *tested* models as a whole describes the observed data best. It, however, does not yield any information about the goodness of a fit or if a model is at all physically reasonable (a comprehensive review on the topic of information-theory based statistical inference can be found in [21]). Furthermore, it does not allow to make any statements about the significance of a specific model parameter (e.g. if an exponential cut-off for a specific component is significant). When using this approach, it is therefore important to carefully design the candidate model collection with physically motivated and reasonable combinations of components and parameters while separately investigating the goodness of fit.

[1] See https://docs.gammapy.org/1.0/user-guide/stats/fit_statistics.html for details.

[2] More information on the AIC and other information criteria can be found in [19–21] and references therein.

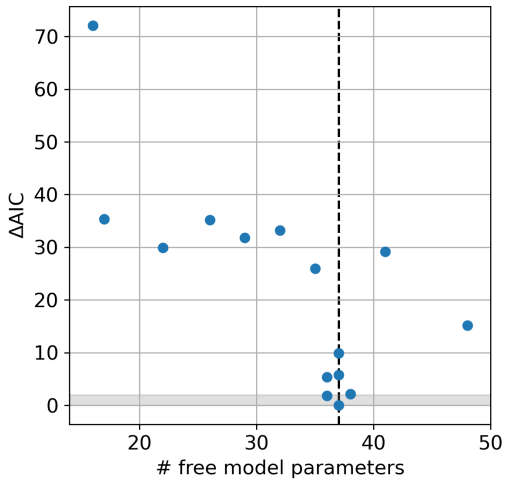

Figure 1: Evolution of difference in AIC score to the model with the lowest score over the number of free model parameters. The dashed vertical line marks the number of free model parameters that yields the lowest AIC score.

2.3 Modelling the gamma-ray sky around Westerlund 2

For the presented study, a total of 15 different models is tested with two to five potential gamma-ray source components. The components are build up of generalised Gaussian spatial models[3] with either power-law spectral models with (ECPL)[4] or without (PL)[5] an exponential cut-off or log-parabola spectra[6]. Starting with a 2-component model with symmetrical morphologies and power-law spectra (i.e. the previously published model for the TeV emission from [6]), the complexity of the models in the candidate collection is gradually increased by adding components and/or degrees of freedom, which include e.g. eccentricity and orientation angle of spatial models and cut-off energies for power-law spectral models. Parameters which are left free in all models are background normalisation and tilt as well as the reference energies of all components' spectral models. The fit is restricted to only regard a circular region with 0.85° radius around the centre of the sky map.

The AIC values are then calculated for each of the models. Plotting the difference in AIC to the lowest score over the number of free model parameters as shown in Fig. 1 visualises how increasing complexity yields successively lower AIC scores with a minimum being reached around 37 free parameters (dashed vertical line) from where on th AIC tends to increases again. The grey band depicts the region in which models can be regarded as describing the data equally well.

With only one other model yielding a ΔAIC value of just < 2, the model showing the lowest AIC

[3]See https://docs.gammapy.org/1.0/user-guide/model-gallery/spatial/plot_gen_gauss.html for details.

[4]See https://docs.gammapy.org/1.0/user-guide/model-gallery/spectral/plot_exp_cutoff_powerlaw.html for details.

[5]See https://docs.gammapy.org/1.0/user-guide/model-gallery/spectral/plot_powerlaw.html for details.

[6]See https://docs.gammapy.org/1.0/user-guide/model-gallery/spectral/plot_logparabola.html for details.

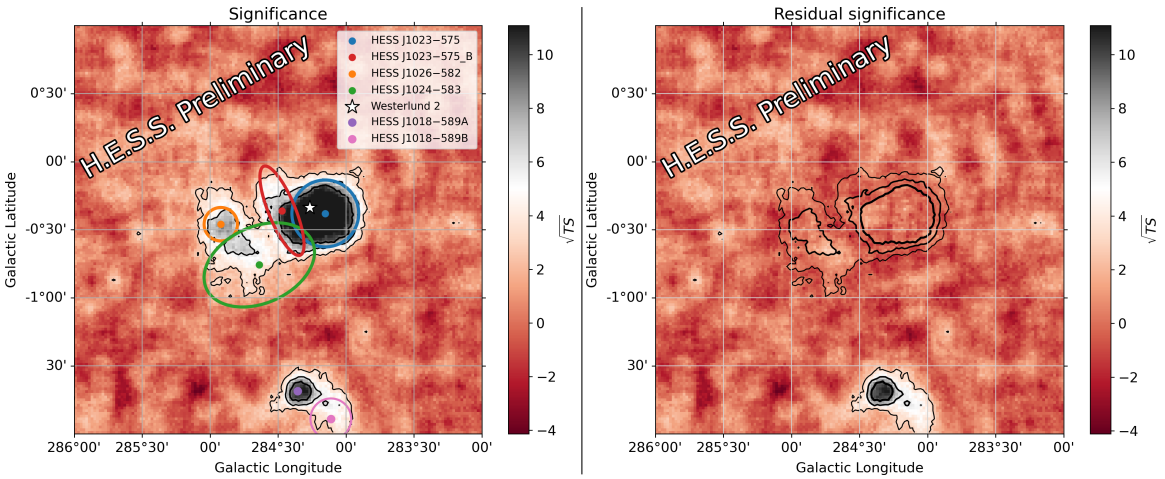

Figure 2: *Left*: Saturated significance map of the Westerlund 2 region for the full dataset, calculated with a disk correlation kernel of 0.1° radius and overlayed with the outlines of the best-fit regions of the preferred model. Black contour lines show 3,6 and 9σ significance levels. *Right*: Residual significance map with the excess predicted by the preferred model removed. As a reference, the original significance contours of the full dataset are shown. It can be seen that the residual shows no imprint of model components.

score is chosen as the preferred model. This model contains four components of which the regions are depicted as coloured shapes in the significance map of the full dataset over all energy bins in Fig. 2 *left*. Fig. 2 *right* shows the residual significance map after subtracting the modelled gamma-ray emission. The residuals in the region of the source complex blend in with the surrounding background fluctuations without showing imprints of the model morphologies, suggesting a well fitting model.

2.4 Preferred model details

The four components of the preferred model as depicted in Fig. 2 *left* are all modelled with generalised Gaussians and PL or ECPL spectra. While all components are extended, their spatial emission profiles differ with HESS J1023−575_B and HESS J1024−583 showing a disk-like morphology with a sharp edge, HESS J1023−575 tending towards a disk-like morphology with a smooth edge and HESS J1026−582 showing a Laplace-like morphology, i.e. a radial exponential emission profile peaking at the centre. Using an independent data calibration and reconstruction chain, significant emission with compatible spectra is found in the four component regions, confirming the results.

As the spectral indices of HESS J1023−575 and HESS J1023−575_B agree within statistical uncertainties and the components show a substantial spatial overlap, the flux per energy bin of these two components is added and an ECPL spectrum is fitted to present a combined spectrum as shown in Fig. 3 *left*. The spectra of the other two sources, the previously known HESS J1026−582 and the newly discovered source HESS J1024−583, are shown in the *central* and *right* panel of Fig. 3 respectively. The main best-fit parameters of the individual model components are listed in Tab. 1.

Overlaying the preferred model components with HI radio data from the Southern Galactic Plane Survey (SGPS) [22, 23] integrated in the 24 – 32 km/s velocity range as depicted in Fig. 4,

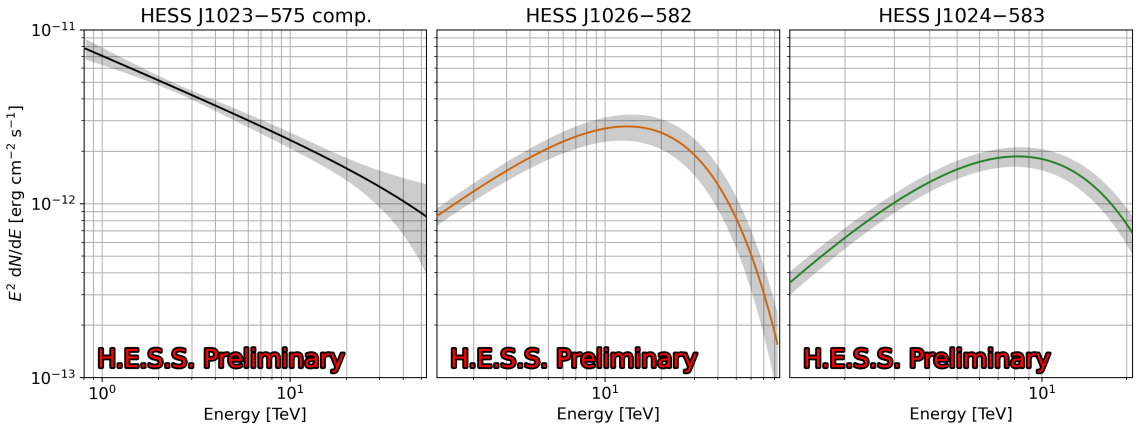

Figure 3: Best fit spectra of the preferred model components. For HESS J1023−575, a compound spectrum is generated by combining the flux estimates of HESS J1023−575 and HESS J1023−575_B and fitting the result with an ECPL spectrum as shown on the *left* panel. The *centre* and *right* panels show the best-fit ECPL spectra for the other two components from the 3D fit.

	HESS J1023−575	HESS J1023−575_B	HESS J1026−582	HESS J1024−583
gal. lon. [deg]	284.15 ± 0.01	284.47 ± 0.01	284.92 ± 0.01	284.64 ± 0.01
gal. lat. [deg]	−0.38 ± 0.01	−0.36 ± 0.01	−0.46 ± 0.01	−0.76 ± 0.01
r_0 [deg]	0.25 ± 0.01	0.35 ± 0.01	0.12 ± 0.01	0.43 ± 0.01
e	-	0.96 ± 0.01	-	0.75 ± 0.02
φ [deg]	-	22.39 ± 0.83	-	113.86 ± 4.26
η	0.22 ± 0.07	0.01± < 0.001	1.00± < 0.001	0.01± < 0.001
E_0 [TeV]	0.99 ± 0.17	1.98 ± 0.13	0.99 ± 0.02	1.06 ± 0.38
Φ_0 [10^{-12} TeV/(s cm^2)]	3.45 ± 0.98	0.18 ± 0.03	0.47 ± 0.06	0.19 ± 0.03
Γ	2.40 ± 0.08	2.52 ± 0.11	1.17 ± 0.05	0.36 ± 0.08
$1/\lambda$ [TeV]	58.01 ± 22.05	n.a.	15.84 ± 1.48	5.00 ± 0.38
$\sqrt{\Delta TS}$	28.5	9.5	16.3	9.6

Table 1: Preliminary best-fit parameters with statistical errors of the individual components of the preferred model.

shows that the new gamma-ray source component HESS J1024−583 (green ellipse) spatially aligns with the elongated cloud structure to the south east of Westerlund 2, which is also seen in CO radio data [9, 10]. The component HESS J1023−575 furthermore coincides with a ring-like spherical shell structure as also outlined in [10].

3. Conclusion and outlook

A new and more detailed picture of the TeV emission around the stellar cluster Westerlund 2 has been generated by applying an AIC-based approach to model selection with elaborate multi-dimensional fitting techniques to the extensive H.E.S.S. data on this region of the sky. Besides updated spatial and spectral descriptions of the previously detected sources HESS J1023−575 and HESS J1026−582, a new elongated disk-like source component with an ECPL spectrum with a cut-off at $\sim$ 8 TeV is found that overlaps with an elongated cloud structure seen in HI and CO

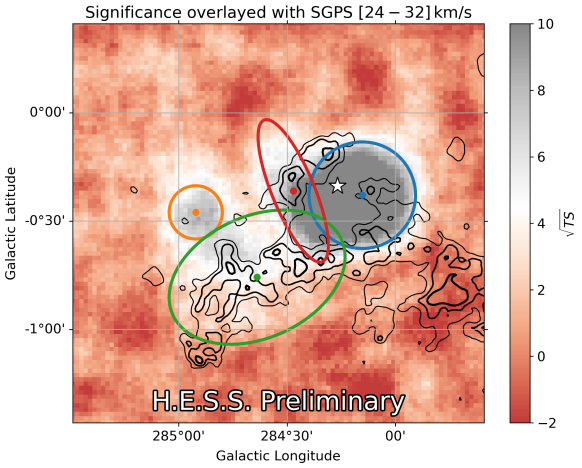

Figure 4: A saturated H.E.S.S. significance map generated with a 0.1° disk kernel over the full energy range is shown in the background. This map is overlayed with [560, 610, 660] K km/s contours (from thin to thick) from HI radio data from the SGPS [22, 23], integrated in the specified velocity range. The preferred model component regions are shown as coloured regions as in Fig. 2 (*left*). The position of the Westerlund 2 cluster is marked with a white star.

radio observations. A detailed interpretation and physical modelling of the whole region in a multi-wavelength context would go beyond the scope of this work and will be subject of a future publication by the H.E.S.S. collaboration.

Acknowledgements

The H.E.S.S. acknowledgements can be found in: https://www.mpi-hd.mpg.de/hfm/HESS/pages/publications/auxiliary/HESS-Acknowledgements-2023.html

References

[1] B. N. Swanenburg et al., The Astrophysical Journal Letters, 243:69-73, 1981, doi:10.1086/183445

[2] C. E. Fichtel et al., The Astrophysical Journal Supplement Series, 94:551–581, 1994, doi:10.1086/192082

[3] C. Pittori et al., Astronomy & Astrophysics, 506(3):1563–1574, 2009, doi:10.1051/0004-6361/200911783

[4] A. A. Abdo et al., The Astrophysical Journal Supplement Series, 183(1):46–66, 2009, doi:10.1088/0067-0049/183/1/46

[5] F. Aharonian et al., Astronomy & Astrophysics, 467(3):1075–1080, 2007, doi:10.1051/0004-6361:20066950

[6] H. E. S. S. Collaboration et al., Astronomy & Astrophysics, 525:A46, 2011, doi:10.1051/0004-6361/201015290

[7] T. L. Holch et al., Journal of Physics: Conference Series, 2398:012017, 2022, 10.1088/1742-6596/2398/1/012017

[8] T. L. Holch, PoS(ICRC2023)779, doi:10.22323/1.444.0779

[9] Y. Kukui et al., Publications of the Astronomical Society of Japan, 61, 4:L23–L27, 2009, 10.1093/pasj/61.4.L23

[10] N. Furukawa et al., The Astrophysical Journal, 781(2):70, 2014, doi:10.1088/0004-637x/781/2/70

[11] H.E.S.S. Collaboration et al., Astronomy & Astrophysics, 612:A1, 2018, doi:10.1051/0004-6361/201732098

[12] H.E.S.S. Collaboration et al. , Astronomy & Astrophysics, 541:A5, 2012, doi:10.1051/0004-6361/201218843

[13] A. M. Hillas, Proceedings of the 19th International Cosmic Ray Conference, 3, 445–448, La Jolla, 1985

[14] S. Ohm et al., Astroparticle Physics, 31:383–391, 2009, doi:10.1016/j.astropartphys.2009.04.001

[15] C. Nigro et al., Universe, 7(10):374, 2021, doi:10.3390/universe7100374

[16] C. Deil et al., 35th International Cosmic Ray Conference (ICRC2017), 301, 766, 2017, doi:10.22323/1.301.0766

[17] D. Berge et al., Astronomy & Astrophysics, 466:1219–1229, 2007, doi:10.1051/0004-6361:20066674

[18] H. Akaike, In: Parzen, E., Tanabe, K., Kitagawa, G. (eds) Selected Papers of Hirotugu Akaike. Springer Series in Statistics., p199–213, Springer, New York, NY, 1998, doi:10.1007/978-1-4612-1694-0_15

[19] J. E. Cavanaugh and A. A. Neath. WIREs Computational Statistics, 11(3):e1460, 2019, doi:10.1002/wics.1460

[20] K. P. Burnham et al., Behavioral Ecology and Sociobiology, 65(1):23–35, 2010, doi:10.1007/s00265-010-1029-6.

[21] R. Mundry, Behavioral Ecology and Sociobiology, 65(1):57–68, 2011, doi:10.1007/s00265-010-1040-y

[22] N. M. McClure-Griffiths et al., The Astrophysical Journal Supplement Series, 158(2):178–187, 2005, doi:10.1086/430114

[23] M. Haverkorn et al., The Astrophysical Journal Supplement Series, 167(2):230–238, 2006, doi:10.1086/508467